

TOPOGRAPHIC MAP GENERATION IN HIGH MOUNTAINOUS AREAS BY MEANS OF InSAR DATA

Thomas Damoiseaux

Aero-Sensing Radarsysteme GmbH
c/o DLR Oberpfaffenhofen
82234 Weßling, Germany
Phone/Fax: +49-8153-281542/-281543
Email: thomas.damoiseaux@dlr.de

Technische Universität Dresden
Fakultät Forst- Geo- und Hydrowissenschaften
Institut für Kartographie

Abstract

This paper examines to what extent a new approach to the production of maps can be taken using radar remote sensing in the cartography of mountainous areas. This will be analyzed with a test area of the Bavarian Alps, Germany. The basis are high resolution, In-SAR data from the airborne AES-1 sensor. After data preparation the information is extracted from the multi-frequency and multi-temporal data with the aim of making topographic maps. These products are then compared with requirements for the high-mountain cartography, and the contribution that radar remote sensing can make to the high-mountain cartography is assessed.

1. Introduction

The goal of a topographic map is that it reflects the nature of the landscape with its characteristic geomorphological elements. These elements should be illustrated in a map as true to form and as vividly as possible. In general data from aerial photography systems and optical remote sensing as well as from terrestrial topographic ground surveys serve as a basis for map production.

This paper analyzes to what extent and with which methods radar remote sensing is able to achieve that aim of a topographic map. The imaging of the ground surface by means of radar systems with synthetic aperture (SAR) generates first a two-dimensional map of the illuminated area. In addition, with the help of the methods of SAR interferometry (InSAR), the ground surface can be reproduced in three dimensions. The SAR images, the coherence image and the digital elevation model (DEM) now serve as a basis for extracting information from the radar data. From this information a model of the real world is generated which then describes reality as well as possible so that cartographic products can be derived from it.

To achieve this goal the methods of digital image processing and pattern recognition are used. One can describe the land cover of the given area and the altitude information in form of contour lines. Land cover and contour lines are then examined with the help of a ground-truth data set to control their accuracy. In a further step they are measured against topographic mapping criteria for high mountains. Finally a statement can be made in regard to the quality of the maps rendered from InSAR data on various scales.

The paper is structured as follows: Chapter 2 treats the InSAR principles, while chapter 3 outlines the processing chain of making topographic maps. In chapter 4 an overview of the AES-1 sensor is given and chapter 5 handles the theory of information extraction. Chapter 6 deals with the application to a concrete area and discusses the results. In the conclusion a view to the future of the project is given.

2. InSAR Principles

Active microwave systems work in the frequency range of 0.3 to 300 Ghz [Ulaby et al, 1981], which corresponds to a wavelength range of 1 m to 1 mm. In this frequency range clouds and rain can be penetrated almost without any hindrance. As the high-frequency pulses are emitted by the sensor itself, the system works with its own illumination and is independent of daylight.

The imaging of a ground surface by means of a SAR system generates a two-dimensional map of the illuminated area. Here a distinction has to be made between the two dimensions, i.e. on one hand the azimuth direction, which is the direction of flight, and on the other hand the range direction, which runs perpendicular to the direction of flight or parallel to the sight of the antenna (Figure 1).

The azimuth resolution depends on the length of the antenna and is therefore limited when using a radar with a real aperture. The SAR technique [Oliver et al, 1998] is used to synthesise a very long antenna by combining signals (echoes) received by the radar as it moves along a track. The synthetic aperture can be constructed by moving a small antenna to different positions through the whole length of the synthetic aperture. At each position a pulse is transmitted. Then the return echoes pass through the receiver and are recorded in an 'echo store'. The range resolution is obtained by a short radar pulse or equivalent techniques.

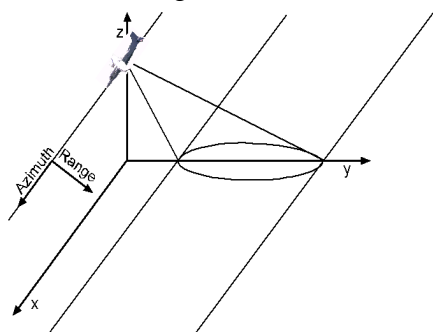


Figure 1. Imaging technique

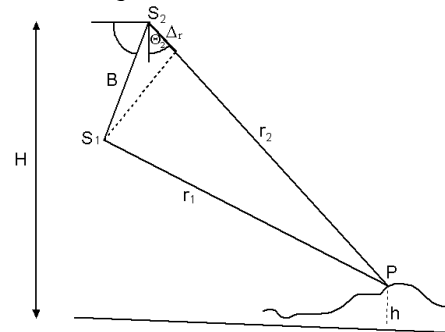


Figure 2. SAR interferometry

Some important imaging properties of SAR appear due to the side looking geometry, namely layover and shadow effects. We can describe them as follows:

Layover: The angle of inclination of the slope facing the sensor becomes greater than the angle of incidence. Information starts to overlap, which no longer permits a clear allocation of the signals (see area AB in Figure 3).

Shadow: Radar shadow arises if the angle of inclination of the slope facing away from the sensor becomes greater than the angle of incidence. Areas occluded by the relief are not visible (see area CD in Figure 4).

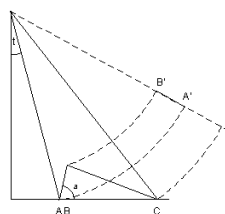


Figure 3. Layover

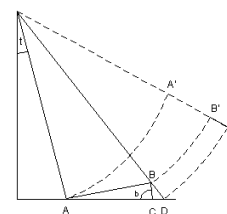


Figure 4. Shadow

A SAR image is generated by processing the recorded raw data [Curlander et al, 1991]. In the processing stage the raw data are range and azimuth compressed forming a two dimensional image in slant range (radar) geometry.

SAR images in slant range need to be projected into a certain cartographic system. For this procedure the DEM information is mandatory. We take advantage of the coherence capability of the radar for doing an interferometric processing by using a second antenna. As in stereometry the height can be evaluated if the same area is imaged from two different directions. On the other hand interferometry [Gens et al, 1996] considers the phase of the signal and not the amplitude like stereometry. By measuring the phase, one gets a very accurate surface model that is independent of the area contrast. By measuring the phase difference of the two SAR images ($\Psi_1 - \Psi_2$) obtained from S1 and S2 (Figure 2), one can determine the range difference $\Delta_r = (r_1 - r_2)$ between the two antennas very accurately as follows:

$$\Delta_r = \frac{\lambda}{4\pi} \cdot (\Psi_1 - \Psi_2) \tag{1}$$

The advantage of measuring the phase is that one can obtain Δ_r within tenth of mm accuracy and also independent of the image contrast, i.e. the surface model of ice or water surfaces is also obtainable.

The height of a point P (cf. Figure 2) can then be derived from Δ_r by

$$h = H - (r_1 + \Delta_r) \cos \Theta_2 \tag{2}$$

H denotes the altitude of antenna S2 above the geoid.

Another helpful feature of InSAR is the evaluation of the coherence. The coherence gives a measure of how identically the backscatter signal is returned to the antennas. Considering targets with a volumetric scattering effect, the backscattered signal of the two antennas will be not identical, i.e. the phase without the contribution of Δ_r and amplitude are not exactly the same, causing a decrease in the coherence. The coherence is defined as:

$$\hat{\gamma} = \frac{\sum_{n=1}^N c_1^{(n)} \cdot c_2^{*(n)}}{\sqrt{\sum_{n=1}^N |c_1^{(n)}|^2 \cdot \sum_{n=1}^N |c_2^{(n)}|^2}} \tag{3}$$

where $c_{1,2}$ = complex 2 dimensional images of the antennas 1 and 2; N = number of averaged samples

3. Processing chain from raw data recording to topographic map

Figure 5 gives overview of how a topographic map is derived. The raw data recording is followed by the SAR and interferometric processing. The geocoding results in a DEM, an ortho SAR image and an ortho coherence image. These results are also called primary features. The step of information extraction then leads to a classification result, contour lines and finally to a topographic map.

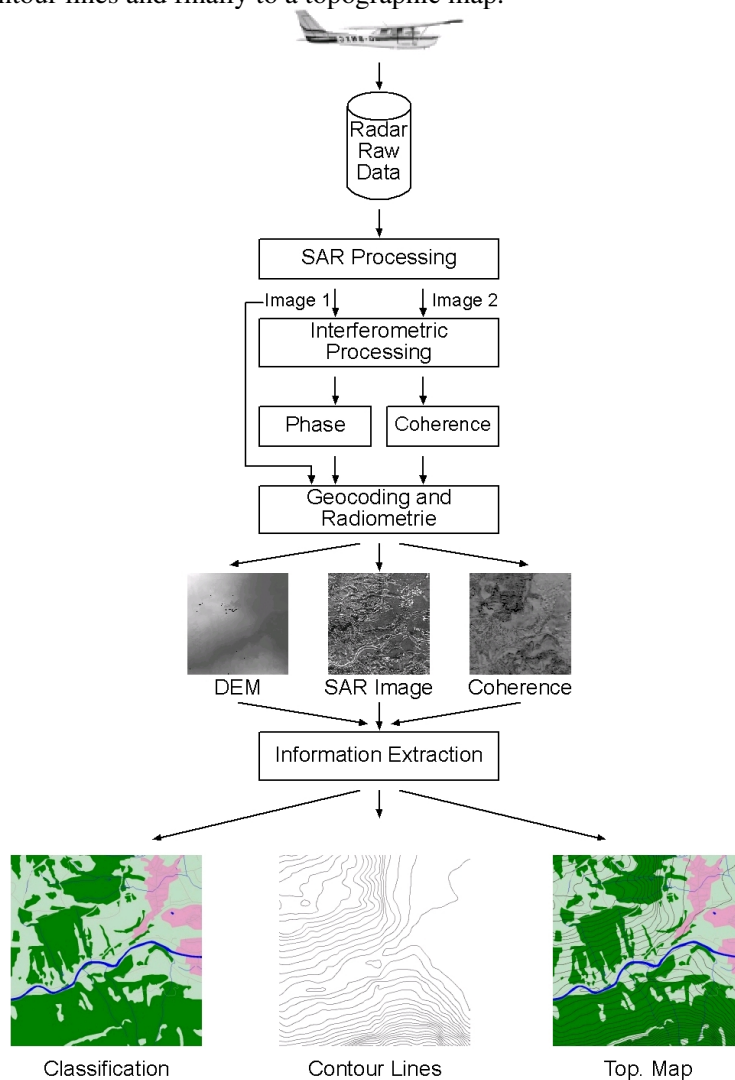


Figure 5. The processing chain from raw data to topographic map

4. The high resolution airborne interferometric SAR AES-1

The data for this work were acquired with the high resolution airborne interferometric SAR AES-1, built and operated by Aero-Sensing Radarsysteme GmbH. The main system parameters of the AES-1 radar are summarized in table 1.

	X-Band	P-Band
operating frequency	9.35 - 9.75 GHz	380 - 450 MHz
polarisation	HH	HH
system bandwidth	400 MHz	70 MHz
pulse repetition frequency	16 kHz	16 kHz
ground resolution (range x azimuth)	0.5 m x 0.5 m	2.5 m x 0.5 m
flight velocity	50 -200 m/s	50 -200 m/s
flight altitude above sea level	500 m - 12000 m	500 m - 12000 m

Table 1. System parameters of the AES-1 radar

5. Information Extraction

The model of the real world gained from the SAR overflight (two antiparallel flight directions) should describe the reality regarding surface coverage and the height information as well as possible. The illustration below (Figure 6) shows the simplified process chain from an image of the real world to a classification result.

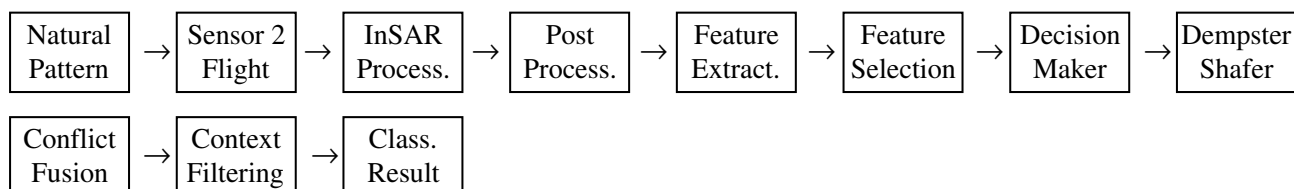


Figure 6. Process chain from a natural pattern to a classification result

After the InSAR processing the data are prepared for the information extraction; this step is called post-processing. At first the X-band image is processed with a Lee filter [Lee, 1981] in order to reduce the speckle. A further step entails geocoding and radiometric correction of the scenes [Holecz, 1993]. Since these processes are dependent on a DEM, it has to be generated in the required cartographic reference system at the beginning of the process. So far the following products, also called primary features, are available for an image analysis:

- SAR image
- DEM
- Coherence image

The primary features, however, are not sufficient if the SAR images are to be interpreted adequately. In order to improve the model, additional information is derived from the primary features. This step is called feature-extraction [Dutra et al, 1998]. In it new features are obtained which are extracted with the help of a texture analysis of the SAR image(s) and the coherence. These features contribute significantly to the improvement of the classification result [Schistad Solberg et al, 1997].

Texture can be analysed in different ways:

- Local Statistics Features
- Co-occurrence matrices [Haralick et al, 1973]
- Laws filter [Laws, 1980]

All features obtained by feature extraction now form a d-dimensional feature space. If d is high, the problem arises that the accuracy of the classification decreases. This phenomenon is known as “curse of dimensionality” [Bishop, 1995]. Therefore the best subset of m features from the set of d possible features must be found, where $m < d$ [Dutra et al, 1998], [Huber et al, 1998]. For this the Jeffreis-Matusita distance (JMD) [Swain et al, 1978] can be used, which makes a statement on the statistical separability of n classes in a feature space between multivariate Gauss distributions. Although most of the features are not Gauss distributed, the JMD can nevertheless be used as a measure of the separability.

The aim is now to derive the likelihoods l_1 for each desired class and each pixel p at the position (x, y) from the m -feature subset. This will be done separately for exactly the same cutting of each flight direction. For this a multivariate Gaussian maximum likelihood classifier (MLC) [Swain et al, 1978] is used.

Now one can fuse the likelihoods l_1 with their appropriate coherence using the Dempster-Shafer Theory of Evidence (DSTE) [Klein, 1993] to get new likelihoods l_2 and a weight of conflict k for each pixel p . Substantially this method is based on collecting data (likelihoods l_1 , coherence) to solve a certain problem (land cover classification) by assigning probabilities to the data and fusing them with the DSTE to obtain a more exact overall probability. The coherence is used here as an expert knowledge. Coherence can be divided into stable land cover, such as man-made or bare soil, and unstable land cover, such as water, forest or agricultural areas. In this connection the coherence can support or dilute the likelihoods l_1 of the different classes and so contribute to more exact likelihoods l_2 .

With a conflict-weighted method one can fuse l_2 and k from each flight direction to a new set of likelihoods l_3 for each pixel p . By using two different flight directions for the classification one can so minimize the influences of the relief on the SAR-specific recording geometry.

The likelihoods l_3 can finally be improved with an algorithm including the context (Potts model) [Besag, 1986] of a pixel p .

In the end the above algorithm leads to the classification result which is a necessary base for a topographic map.

As a next step one had to extract height information in form of contour lines from the DEM as shown in Figure 7.



Figure 7. Process chain from a natural pattern to contour lines

The DEM developed with the help of the SAR interferometry is now the basis for the height information. Before one can extract the contour lines following aspects have to be taken into account:

- Typical InSAR mistakes (phase-unwrapping) have to be analysed and minimised.
- Optimum mosaiking between the two different flight directions and overlapping tracks have to be performed.
- Since we have only information from the surface (X-Band) and not from the ground we have to estimate the height of trees, houses and other features. These heights have to be deduced from the DEM in order to have the exact height levels from the ground.
- To smooth the DEM some filter operations have to be performed.

Now the contour lines can be extracted.

As Figure 8 shows the topographic map information is a combination between the classification result and the contour lines in a certain equidistance. Both pieces of information are the result of the information extraction from interferometric SAR data.

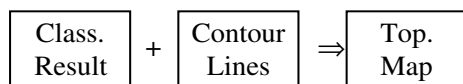


Figure 8. Generating topographic maps

6. Mapping the Edelsberg area

The Edelsberg area belongs to the Bavarian alpine foothills [Hofmann, 1970] with three different geomorphological units:

- the flysch zone of the Edelsberg
- the Helvetikum to the north of the Edelsberg
- the northern border of the Lime Alps in the south of the Edelsberg

For the classification one can use as input the X- (cf. Figure 9 and 10) and P-Band scene from the two different directions.

After feature extraction and feature selection the m-feature subsets from each direction are classified with the MLC into three different classes:

- forest (dark green) - man-made (light green) - open area (red)

which leads to the likelihoods l_1 (Figure 11). With the DSTE the likelihoods l_1 and the appropriated coherence (Figure 12) are fused to new likelihoods l_2 (Figure 13) and a map with the conflicts k (Figure 14). Figure 15 shows the new likelihoods l_3 as a result of the conflict-weighted fusion. The final result (Figure 16) can then be compared to a ground truth from ATKIS-Data (© BLVA München) (Figure 17).

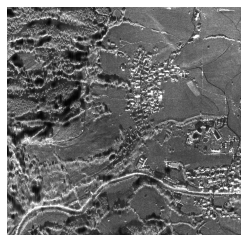


Fig. 9. X-Band east-west

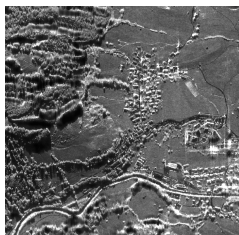


Fig. 10. X-Band west-east

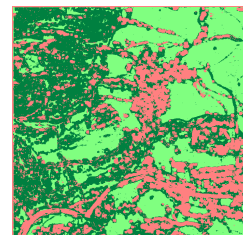


Fig. 11. Likelihoods l_1

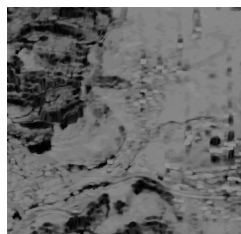


Fig. 12. Coherence

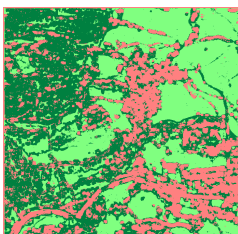


Fig. 13. Likelihoods l_2

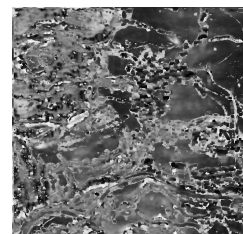


Fig. 14. K map

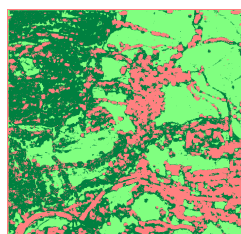


Fig. 15. Likelihoods l_3

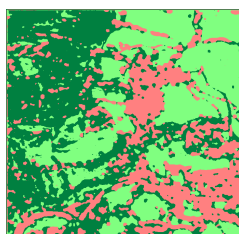


Fig. 16. Final result



Fig. 17. ATKIS-data

In the Figures 18 and 19 a comparison in form of profiles is made between the ATKIS (© BLVA München) reference DEM and a DEM generated by SAR interferometry.

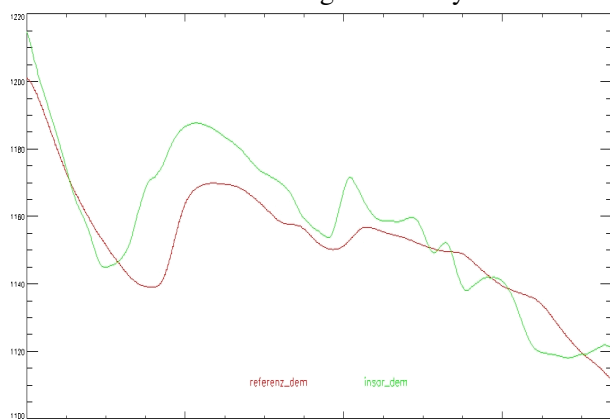


Figure 18. Profile1

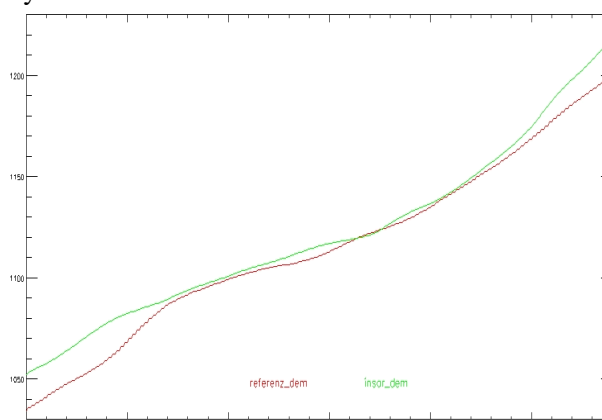


Figure 19. Profile2

The results presented lead to the following conclusions:

a. Classification result

- settlement areas are detected well
- since settlement areas and layover areas have a similar spectral signature, layover areas are wrongly classified as settlement areas
- linear elements (roads, rivers) occur in the classification often at the edge of a forest, meadow or settlement
- detection of rivers is poor
- forest, meadow and settlement can otherwise be separated well

So it has been shown that at least three different classes can be extracted from the dataset with the presented classification algorithm. One or two further classes could also be derived with this algorithm. If we assume four to five different classes, low- and high-mountain terrain can be described sufficiently well with respect to its surface coverage. This provides a useful basic structure for producing topographic maps. It can thus be stated that radar remote sensing can provide a description of surface coverage which is necessary for producing topographic maps.

b. Height accuracy

The profiles in Figures 17 and 18 compare the ATKIS (© BLVA München) reference DEM to the InSAR DEM. Profile 1 run from west to east while profile 2 run from south to north.

Through the comparison the following matters become obvious:

- the geomorphological landforms will be observed in both profiles
- the InSAR DEM sometimes shows more details than the reference (Profile1)
- in some fields the profiles from the InSAR DEM differ from the reference. One reason could be a wrong estimation of the height of the trees, a too strong/weak filtering of the DEM or unwrapping mistakes.

The next step in the analysis is to improve the DEM with the already mentioned methods. Further characteristic geomorphological parts from the area will then be examined exemplarily. Finally a statement can be made if the landscape form can also be described accurately enough for cartography purposes in respect to the extracted contour lines.

7. Conclusions

The status of information extraction from InSAR data for map production was shown. The next step is to improve the DEM so that the contour lines can be extracted from it. The classification result and the contour lines are then checked for their accuracy. The cartographic result then describes the combination of contour lines and surface coverage. These will be examined against the criteria of high-mountain cartography on different scales. Finally a statement can be made as to which landscape form (low- and high mountain) up to which scale can be described cartographically accurately and reasonably with the help of SAR data. In the near future the data from two Austrian high-mountain areas, the Silvretta area and an area around Galtür, will be prepared and processed with the same algorithm as presented here.

References

- Besag, J. (1986).
On the Statistical Analysis of Dirty Pictures.
Journal of the Royal Statistical Society,
Series B, 48(3):259-302.
- Bishop, Ch. (1995).
Neural Networks for Pattern Recognition.
Clarendon Press, Oxford.
- Curlander, J.C., and Mc Donough, R.N. (1991).
Synthetic Aperture Radar, System & Signal Processing.
John Wiley & Sons.
- Dutra, L.V., and Huber, R. (1998).
Feature Extraction and Selection for ERS-1/2
InSAR Classification.
International Journal of Remote Sensing,
Vol. 20, No. 5, pp. 993-1016, March 1999.
- Gens, R., and van Genderen, J.L. (1996).
Review Article SAR interferometry-issues, techniques,
applications.
International Journal of Remote Sensing,
VOL. 17, No. 10, 1803-1835.
- Haralick, R.M., Shanmugan, K., and Dinstein, I. (1973).
Textural features for image classification.
IEEE Transactions on Systems, Man and Cybernetics,
Vol. SMC-3, 610-621.
- Hofmann, W., and Louis, H. (Ed.) (1970).
Alpen Nördliche Flysch- und Kalkalpen Kartenprobe 1:
Formen im Flysch, begrenzt von schärferen Formen im
Kalk, Edelsberg, westlich Pfronten im Allgäu.
Georg Westermann Verlag
- Holecz, F. (1993).
Postprocessing von SAR-Satellitenbilddaten.
Remote Sensing Laboratories, Department of Geography,
University of Zurich.
- Huber, R., and Dutra, L.V. (1998).
Feature Selection For ERS-1/2 InSAR Classification:
High Dimensionality Case.
Proceedings of International Geoscience and Remote
Sensing Symposium, Seattle, WA, USA, July 1998.
- Klein, L. (1993).
Sensor data fusion concepts & applications.
SPIE, Bellingham, WA, USA.
- Laws, K.I. (1980).
Textured image segmentation.
USCIP Report 940, Image Processing Institute
University of Southern California.
- Lee, J.S. (1981).
Refined Filtering of Image Noise Using Local Statistics.
Computer Graphics and Image Processing 15, 380-389.
- Oliver, C., and Quegan, S. (1998).
Understanding Synthetic Aperture Radar Images.
Artech House, Boston & London.
- Schistad Solberg, A.H., and Jain, A.K. (1997).
Texture Fusion and Feature Selection Applied to SAR
Imagery.
IEEE Transactions on Geoscience and Remote Sensing,
Vol. 35, No. 2.
- Swain, P.H., and Davis, M. (1978).
Fundamentals of Pattern Recognition in Remote
Sensing.
McGraw-Hill.
- Ulaby, F.T., Moore, R.K., and Fung, A.K. (1981,82,86).
Microwave remote sensing: active and passive, Vol. I-III,
Artech House, Boston & London.
- ATKIS-Data
Bayerisches Landesvermessungsamt München (Ed.).
Digitale Daten aus dem Amtlichen Topographisch-
Kartographischen Informationssystem des Bayerisches
Landesvermessungsamtes (BLVA).